JOURNAL OF SOLID STATE CHEMISTRY **138,** 135–140 (1998)
ARTICLE NO. SC987764

A HRTEM Study of the Ruddlesden–Popper Compositions $Sr_2LnMn_2O_7$ (*Ln* = Y, La, Nd, Eu, Ho)

J. Sloan,*,† P. D. Battle,*,[1] M. A. Green,* M. J. Rosseinsky,*,[1] and J. F. Vente*

*Inorganic Chemistry Laboratory, University of Oxford, South Parks Road, Oxford, OX1 3QR, United Kingdom; and †Department of Materials, University of Oxford, Parks Road, Oxford, OX1 3PH, United Kingdom

Received October 6, 1997; in revised form January 20, 1998; accepted January 21, 1998

High resolution transmission electron microscopy has been used to probe the microstructure of the $n = 2$ Ruddlesden–Popper manganates $Sr_2LnMn_2O_7$ (*Ln* = Y, La, Nd, Eu, Ho). Intergrowths of $n = 1$ (K_2NiF_4) are observed only for *Ln* = La. Intergrowths with $n \geq 5$, essentially perovskite microdomains, are seen in the other compositions. The density of perovskite regions is greatest near the edges of the thin specimens, with the $n = 2$ structure becoming established in the bulk. The complementarity of HRTEM and neutron diffraction is discussed.

INTRODUCTION

The observation of colossal magnetoresistance (CMR) just above the Curie temperatures (T_c) of the pseudo-cubic perovskites $Ln_{1-x}Ae_xMnO_3$ (*Ln* = lanthanide, Bi; *Ae* = Ca, Ba, Sr, Pb) has attracted considerable attention (1–5). All of these manganates have an insulating, high-temperature paramagnetic phase and a metallic, low-temperature phase which shows a spontaneous magnetization. Similar electronic behavior has been observed in the oxide $(Sr_{1.8}La_{1.2})Mn_2O_7$, which also shows CMR around T_c (6). The latter material belongs to the Ruddlesden–Popper (7) (RP) family of compounds, as indeed do the perovskites referred to above. RP phases have the general formula $A_{n+1}B_nO_{3n+1}$ and they consist of perovskite (ABO_3) blocks, n octahedra thick, which are bordered by rock-salt (AO) layers. $(Sr_{1.8}La_{1.2})Mn_2O_7$ (Fig. 1) is an $n = 2$ compound, where the perovskite structure is the $n = \infty$ end member. It has been shown that the magnetotransport behavior of the $n = 2$ compounds is very sensitive to the Sr : Ln ratio and to the exact chemical nature of *Ln*. Samples of $Sr_{2-x}Nd_{1+x}Mn_2O_7$ ($0 \leq x \leq 0.2$) have shown CMR (8, 9), albeit in the absence of ferromagnetic ordering, as has $Sr_{1.8}Pr_{1.2}Mn_2O_7$ (8). However, no CMR was detected in $Sr_2YMn_2O_7$ (10). The structural chemistry of these materials has been studied extensively by neutron diffraction and, in many cases, the results of these experiments have revealed unexpected complexities. Mitchell *et al.* (11) refined the crystal structure of $Sr_{1.8}La_{1.2}Mn_2O_7$ as a function of temperature, but found that they had to allow for the presence of $\sim$10% $(Sr, La)_2MnO_4$, a RP $n = 1$ impurity phase. Battle *et al.* (12) studied a sample of overall composition $Sr_2LaMn_2O_7$ and concluded that it was actually a biphasic mixture of $Sr_{1.8}La_{1.2}Mn_2O_7$ and $Sr_{2.04}La_{0.96}Mn_2O_7$. More remarkably, a sample of $Sr_2NdMn_2O_7$ was found (13) to consist of two $n = 2$ RP phases with the same composition, but with a different distribution of Sr and Nd over the two available crystallographic sites, one in the rock-salt layer and one in the perovskite block. One of the two phases ordered antiferromagnetically at low temperatures, whereas the other appeared to behave as a spin glass. The identification of two phases with very different magnetic properties created the as yet unsolved problem of determining which phase gives rise to the CMR behavior. As a result of a slight rotation of the MnO_6 octahedra, $Sr_2YMn_2O_7$ and $Sr_2HoMn_2O_7$ (14) have a symmetry (space group $P4_2/mnm$) lower than the phases described above ($I4/mmm$). Neither the Ho nor the Y compound shows long-range magnetic ordering at temperatures above 1.5 K, although there is evidence for the formation of a spin glass state (15). It became apparent during the analysis of neutron diffraction data collected on the Y- and Ho-containing samples that both contain a small amount ($\sim$2% by weight) of an $n = \infty$ perovskite phase. The biphasic nature of all the $Sr_2LnMn_2O_7$ samples referred to above suggests that the synthesis of equilibrium compositions may be very complex, and we have shown (16) how apparently minor changes in synthesis conditions can affect the nature of a reaction product. Characterization by neutron diffraction involves the use of a penetrating beam with a wavelength of $\sim$1.5 Å, and the structural studies described above therefore describe the average bulk structure of the particles in our polycrystalline samples. We have now completed a HRTEM study of the same samples in order to

[1]To whom correspondence may be addressed.

0022-4596/98 $25.00

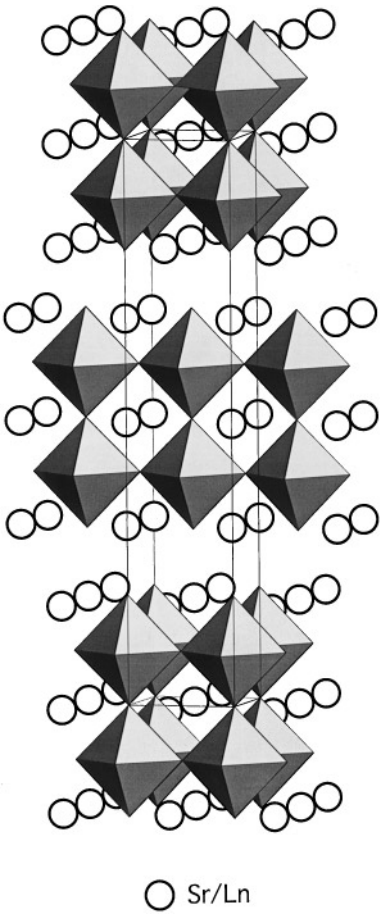

FIG. 1. The crystal structure of $Sr_2LnMn_2O_7$, showing MnO_6 octahedra and Sr/*Ln* atoms.

investigate, using a short wavelength probe, the defects which occur in relatively thin crystallites or close to the edge of larger particles. The results of this study are presented below.

EXPERIMENTAL

The preparation of the samples of $Sr_2LaMn_2O_7$, $Sr_2NdMn_2O_7$, $Sr_2EuMn_2O_7$, $Sr_2HoMn_2O_7$, and $Sr_2YMn_2O_7$ used in this study has been described elsewhere (9, 14, 15, 17, 18). Each microscopy specimen was ultrasonically dispersed in Analar chloroform before being transferred to lacey carbon-coated copper grids (Agar, 200 mesh). HTREM was performed in a JEOL 4000EX electron microscope operated at 400 kV (point resolution = 1.6 Å). All high-resolution images were recorded at or close to optimum Scherzer defocus conditions. Selected specimens were examined using a JEOL 2010 electron microscope fitted with a LINK "Pentafet" energy dispersive X-ray microanalysis (EDX) system which was used to verify compositional homogeneity. For selected high-resolution images, HRTEM multislice image simulations were carried out using the EMS suite of programs (19). The structural parameters used in these calculations were obtained from the refinement of neutron (La, Nd, Ho, Y) or X-ray (Eu) diffraction data, and the microscope parameters used are recorded in Table 1. As a result of the chosen experimental conditions, heavy atoms appear as black spots in the lattice images shown below, and regions of relatively low electron density appear as white spots.

RESULTS

The tetragonal unit cell of the $n = 2$ RP structure has approximate dimensions $4 \times 4 \times 20$ Å; in the case of $Sr_2HoMn_2O_7$ and $Sr_2YMn_2O_7$ a supercell of size $\sim 5.5 \times 5.5 \times 20$ Å is adopted. The most readily interpretable zone axis, [010] of the smaller unit cell, was used for lattice imaging as this allowed for direct comparison of the degree of order from one sample to another. In this context, the word "order" refers to the absence of stacking faults, intergrowths, etc., in the microstructure of the crystallites and not to the distribution of cations over specific crystallographic sites. In general, all phases exhibited both ordered and disordered crystallites, although the extent and nature of the disorder varied from one compound to another. The extent of disorder (i.e., the ratio of ordered to disordered crystallites) observed in the respective phases increased in the sequence.

$$Sr_2LaMn_2O_7 < Sr_2YMn_2O_7 < Sr_2NdMn_2O_7 < Sr_2EuMn_2O_7 < Sr_2HoMn_2O_7.$$

However, even the crystallites which we classify as disordered had large regions ($\sim 95\%$ volume fraction) of unperturbed $n = 2$ RP structure. For all of the well-ordered crystallites, good correspondence was always observed between the observed lattice images (Figs. 2a, 3a, 6a, and 7a) and their simulations (inset). The latter could all be calculated from the same structural model (i.e., Fig. 1), taking into account the relatively small variations in unit-cell parameters from one compound to another. For the purpose of multislice image simulation, therefore, all of the ordered crystals appear to be isostructural. The techniques of HRTEM lattice imaging and multislice image simulation

TABLE 1
HRTEM Parameters for EMS Image Simulation

Accelerating voltage	400 kV
Spherical aberration constant (C_s)	0.9 nm
Semiconvergence angle (α)	0.8 mrad
Objective lens aperture diameter	10 nm^{-1}

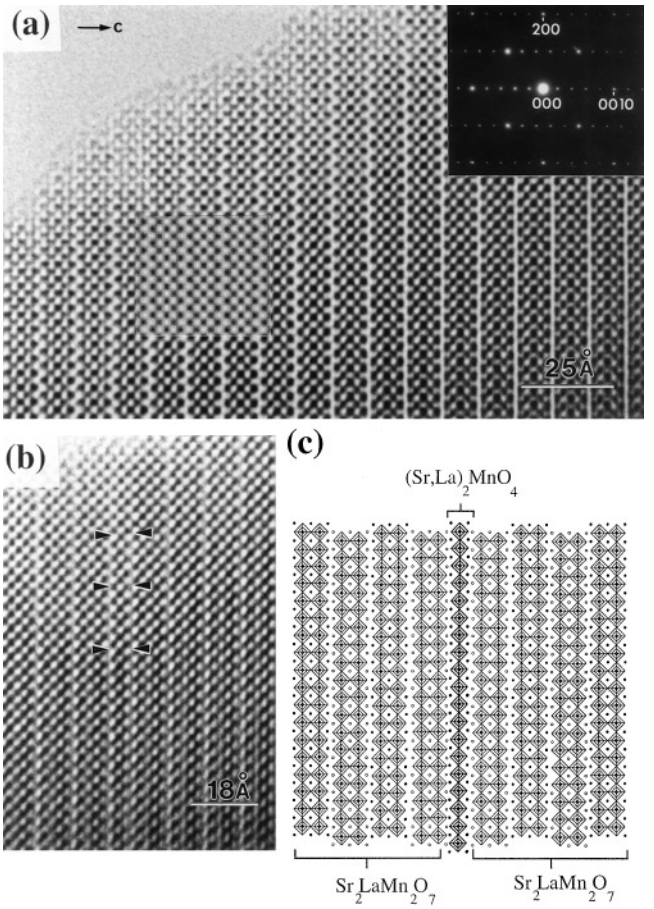

FIG. 2. (a) Diffraction pattern, observed lattice image, and simulated image of an ordered region of $Sr_2LaMn_2O_7$; the simulated image was computed for a 22 Å thick foil at 300 Å defocus. (b) A region of $Sr_2LaMn_2O_7$ containing an $n = 1$ $(Sr,La)_2MnO_4$ defect, indicated by arrows. (c) A schematic representation of the microstructure of (b).

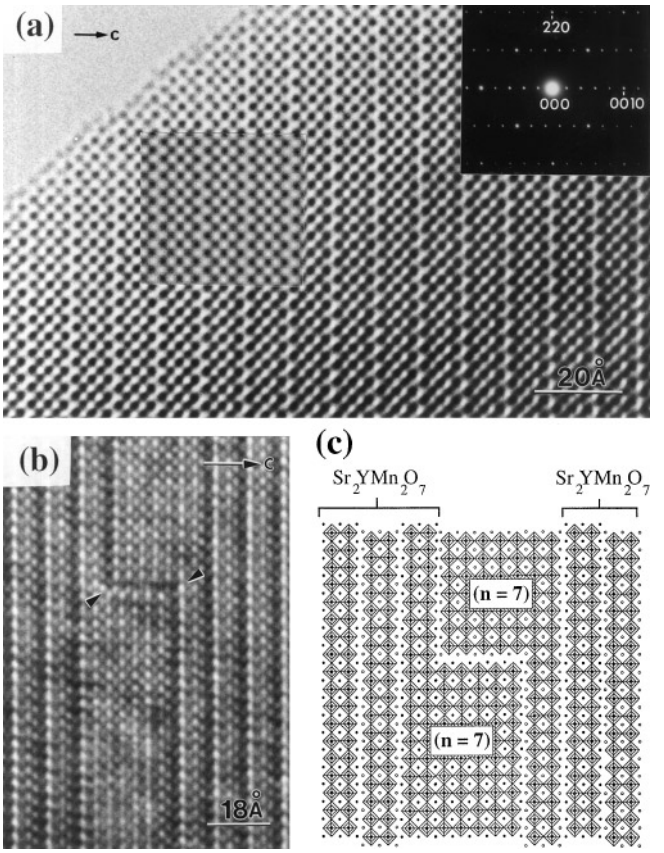

FIG. 3. (a) Diffraction pattern, observed lattice image, and simulated image of an ordered region of $Sr_2YMn_2O_7$; the inset simulated image was computed for a 22 Å thick foil at 300 Å defocus. (b) A relatively thick region of $Sr_2YMn_2O_7$ containing two L-shaped blocks consisting of $n = 7$ layers truncating to $n = 2$ ($Sr_2YMn_2O_7$) layers. The two arrowheads indicate the "step" boundary where the growth sequence is reversed. (c) A schematic representation of the step boundary microstructure in (b).

are not directly sensitive to subtle structural changes, for example the rotation of MnO_6 octahedra that causes $Sr_2YMn_2O_7$ and $Sr_2HoMn_2O_7$ to have a lower symmetry than $Sr_2LaMn_2O_7$, $Sr_2NdMn_2O_7$, and $Sr_2EuMn_2O_7$ (see above). We have, however, indexed the inset electron diffraction patterns of the former two phases (Figs. 3a, 7a, and 7b) in a way which is consistent with their true space group and unit cell. The data from our bulk XRD and neutron diffraction studies (14) provide more reliable information regarding the fine structural variations in this series of materials.

As indicated above, the phase with the lowest defect density, $Sr_2LaMn_2O_7$, exhibited mainly well-ordered crystallites, a typical example of which is shown in Fig. 2a. For this crystallite, order was maintained over a considerably greater volume than indicated by the lattice image, as indicated by the inset diffraction pattern obtained from a larger region of crystal. For other crystals, occasional intergrowth with the lowest member of the $AA'_{n+1}B_nO_{3n+1}$ homologous series (i.e., $n = 1$, effectively K_2NiF_4-type) was also observed. The $n = 1$ layers were invariably observed as isolated, singular lamellae intergrown in bulk crystals of the higher $n = 2$ homologue. An example of this is shown in Fig. 2b together with a schematic representation of the microstructure (Fig. 2c). This kind of intergrowth was observed only for the $Sr_2LaMn_2O_7$ compound.

As with $Sr_2LaMn_2O_7$, the $Sr_2YMn_2O_7$ compound exhibited mainly well-ordered $n = 2$ crystallites, an example of which is shown in Fig. 3a. Order over longer distances is again reflected by the lack of streaking in the inset diffraction pattern. Individual defect lamellae of higher homologues (i.e., of $AA'_{n+1}B_nO_{3n+1}$) were occasionally observed in other crystals with the $n = 7$ homologue being the most common. Figure 3b shows an unusual example of this type of defect, observed for a relatively thick region of crystal. On either side of the micrograph, $Sr_2YMn_2O_7$ layers can be seen although in the middle, a large $n = 7$ lamellae with a prominent "step" can also be seen (arrowed). On either side of the step two intertwining L-shaped blocks of $n = 7$

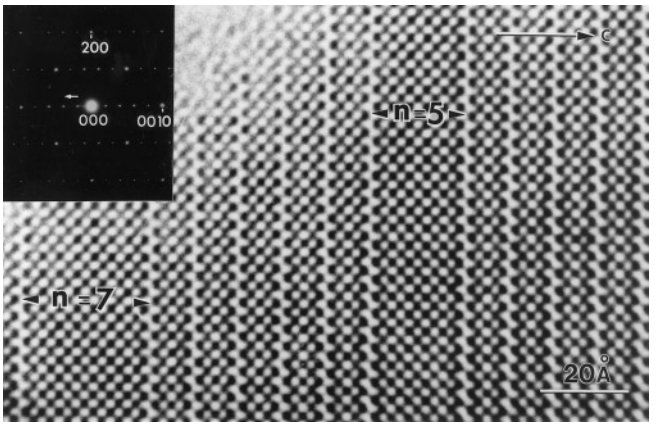

FIG. 4. Image and diffraction pattern of a fragment of $Sr_2NdMn_2O_7$ intergrown with lamellae corresponding to $n = 5$ and $n = 7$. A small amount of streaking, arrowed in the diffraction pattern along [001], indicates the relatively small extent of the disorder in a larger region of the same crystal. The $n = 2$ microstructure is effectively identical to that of $Sr_2YMn_2O_7$ (Fig. 3a).

can be observed in which the $n = 7$ lamellae blocks truncate to $n = 2$. A schematic representation of the defect microstructure is shown in Fig. 3c.

The types of intergrowth encountered for $Sr_2YMn_2O_7$ were generally even more prominent for both $Sr_2NdMn_2O_7$ and $Sr_2EuMn_2O_7$, although with both phases, ordered crystallites were also common. In Fig. 4, a fragment of $Sr_2NdMn_2O_7$ intergrown with lamellae of two separate thicknesses, corresponding to the $n = 5$ and $n = 7$ homologues, can clearly be seen. Streaking in the corresponding diffraction pattern (inset in Fig. 4), arising from this disorder, is also prominent. In Fig. 5a, a type of disorder related to that observed in Fig. 3b for $Sr_2YMn_2O_7$ can be observed. In the micrograph, obtained from a relatively thick region of crystal, two step-like defects are indicated by the arrows **a** and **b**. The second step defect (**b**) occurs at a region where an individual $Sr_2NdMn_2O_7$ lamella, indicated on the right of the micrograph by the arrow **c**, has rotated by 90°, resulting in the demarcation of a block of either $n = 7$ or $(Nd,Sr)MnO_3$ (effectively ABO_3 structure) above the defect and also, in conjunction with the step boundary **a**, a second block below this defect of similar composition. A third block is demarcated below step boundary **a**. This "block" defect was found to extend, in a somewhat random fashion, in both vertical directions beyond the limits of the micrograph and gave rise to rotation streaks (arrowed) in the corresponding diffraction pattern (inset). A schematic representation of the block defects, as they appear in the lower region of the micrograph in Fig. 5a is shown in Fig. 5b. This kind of defect is rare in layered perovskite systems. In Fig. 6a, an ordered crystallite of $Sr_2EuMn_2O_7$, together with an inset diffraction pattern and simulated image, can be seen. In Fig. 6b, a second crystallite of $Sr_2EuMn_2O_7$ exhibiting an $n = 7$ lamellar defect (cf. Fig. 4) is shown.

$Sr_2HoMn_2O_7$ was apparently the most disordered of the five phases studied. Only a few ordered crystallites of the form shown in Fig. 7a were observed, whereas disordered crystallites exhibiting multiple higher homologue lamellae

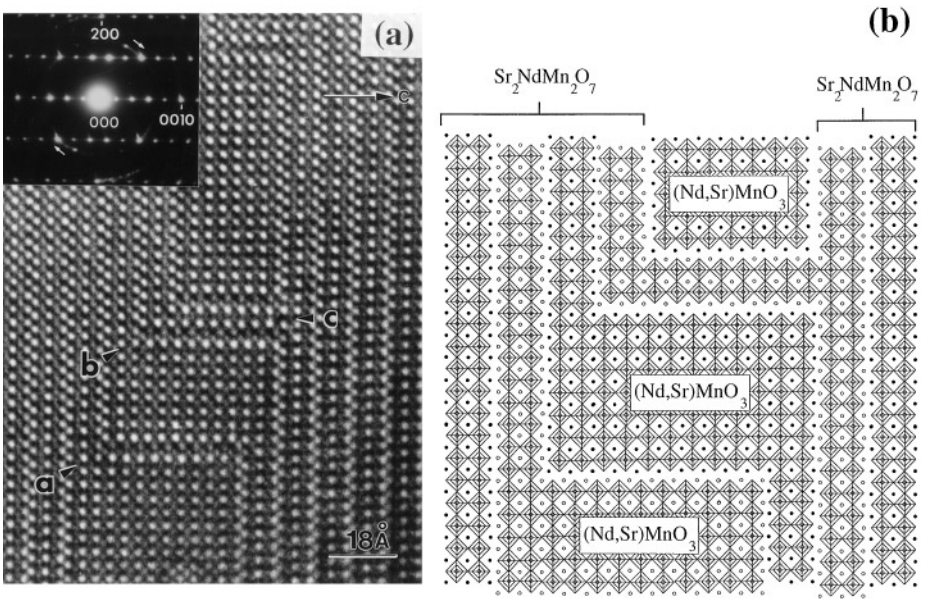

FIG. 5. (a) A region of $Sr_2NdMn_2O_7$ containing $n = 7$ intergrowths, with steps **a** and **b** marked by arrowheads. One of these is caused by a 90° rotation of an entire $n = 2$ lamella (arrow **c**). These defects demarcate blocks with effectively $(Nd,Sr)MnO_3$ composition and give rise to rotation streaks in the inset diffraction pattern. (b) A schematic representation of the microstructure of (a).

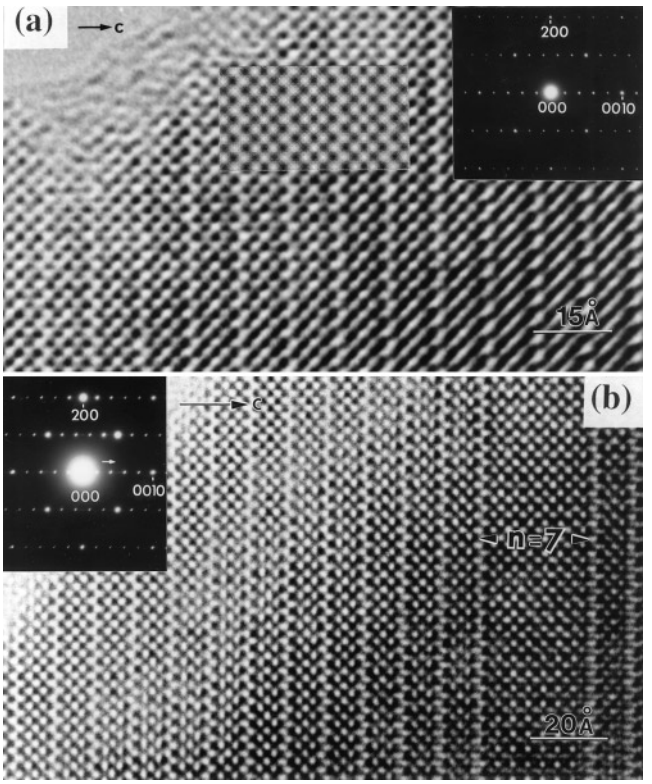

FIG. 6. (a) Diffraction pattern, observed image, and simulated image of an ordered region of $Sr_2EuMn_2O_7$; the simulated image was computed for a 22 Å thick foil at 300 Å defocus. (b) A region of $Sr_2EuMn_2O_7$ containing an $n = 7$ intergrowth (cf. Fig. 4a).

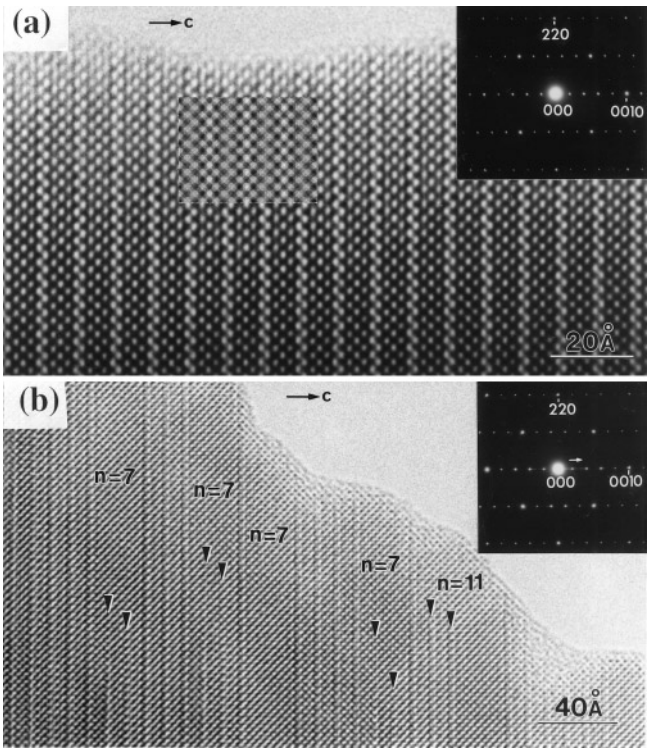

FIG. 7. (a) Diffraction pattern, observed image, and simulated image of an ordered region of $Sr_2HoMn_2O_7$; the simulated image was computed for a 33 Å thick foil at 400 Å defocus. (b) A disordered region of $Sr_2HoMn_2O_7$ showing the intergrowth of $n = 7$, $n = 11$ lamellae, and the dominance of $n = 2$ away from the edge of the specimen.

were frequently observed. Figure 7b shows a typical example. In the micrograph, a number of $n = 7$ lamellae and one $n = 11$ lamellae are intergrown with $Sr_2HoMn_2O_7$. A number of these lamellae exhibit discontinuation fringes as the crystal becomes thicker (arrowed) and the microstructure reverts from the higher homologue defects to $Sr_2HoMn_2O_7$. The random nature of this integrowth is consistent with that observed in other similarly disordered crystals of $Sr_2HoMn_2O_7$.

DISCUSSION AND CONCLUSIONS

The lattice images presented above illustrate the complex microstructure of these materials. Our sample of $Sr_2LaMn_2O_7$ has a low defect density and we did not observe $n = \infty$ perovskite regions. Our previous neutron diffraction study (12) showed that two $n = 2$ RP phases are present in this sample in a ratio of 4 : 1. There is nothing in the micrographs to indicate that two phases are present, but their structures, as refined by neutron diffraction, are so similar that this is not surprising. The well-ordered nature of the sample is consistent with a recent HRTEM study of $Sr_{1.8}La_{1.2}Mn_2O_7$ by Seshadri *et al.* (20), although they did observe $n = \infty$ regions in their sample. The crystallinity of these phases is very sensitive to the conditions of synthesis (10) and the difference in the microstructure of our sample and those of Seshadri *et al.* may be due to their use of a preparative route which utilized a Bi_2O_3 flux. It is important to remember that the disordered crystallites illustrated above were chosen to demonstrate the type of disorder which can occur, and that the defect-rich regions constitute only a small fraction of the whole sample. The relatively low concentration of defects is the most likely reason that no perovskite phase was detected in our neutron diffraction study of $Sr_2NdMn_2O_7$—again, two $n = 2$ phases were identified. Furthermore, many of the defects are too small to give a coherent diffraction pattern in an experiment carried out with a wavelength of ~ 1.5 Å. However, it is also important to remember that neutron and electron beams penetrate the sample to different depths, and some of the apparent inconsistencies may arise because only thin boundary regions of the specimen are studied in the electron microscope, whereas neutron diffraction probes the bulk sample. The two sets of results would be reconciled if the perovskite regions occurred predominantly at the edge of a grain, with the $n = 2$ structure dominating in the bulk. The distinction between local structure and average structure has been

emphazised previously by Laffez *et al.* (21) in discussing the results of their HRTEM study of $Pr_{1.4}Ca_{1.45}Ba_{0.15}Mn_2O_7$. It is less surprising to observe regions of perovskite in $Sr_2YMn_2O_7$ because such a phase was identified in our neutron measurements. It is more surprising to find that $Sr_2HoMn_2O_7$ shows a much higher defect concentration than the Y analogue, because neutron diffraction led us to believe that these two samples were structurally equivalent (14). The images in Fig. 7 do suggest that perovskite regions are more common near the edge of the specimen and that the $n = 2$ structure develops on moving into the crystallite. This is consistent with the point made above, that different radiations probe different regions of the sample, with neutron diffraction sampling the bulk and not just the edge. The micrographs in Fig. 7 show that the explanation offered above in the discussion of $Sr_2NdMn_2O_7$ is certainly valid in the case of $Sr_2HoMn_2O_7$, and the same reasoning explains why the Ho and Y compounds appear similar when studied with neutrons, despite the former showing a greater number of disordered crystallites in HRTEM. However, in view of the fact that we have seen $n \geq 2$ regions in relatively thick crystallites of both $Sr_2NdMn_2O_7$ and $Sr_2YMn_2O_7$, an explanation of the apparent discrepancies between the results from neutron diffraction and HRTEM experiments should probably emphasize the low volume fraction of defects in the sample, remembering that the micrographs presented here illustrate atypical regions, rather than the fundamental differences between the two experiments. The predominance of $n = 7$ perovskite regions in all but the La compound is curious, but the significance of this observation is not clear.

The defects described above are likely to have significant consequences for the magnetotransport properties of these materials. It is likely that grain boundaries play a key role in controlling these properties (22), and this is apparently the region where the local structure differs markedly from the bulk structure determined by neutron diffraction. It is clear that although it is important to understand the properties of the bulk material, it is also important to use electron microscopy to identify departures from the bulk structure.

ACKNOWLEDGMENT

We are grateful to the EPSRC for financial support.

REFERENCES

1. A. Urushibara, Y. Moritomo, T. Arima, A. Asamitsu, G. Kido, and Y. Tokura, *Phys. Rev. B* **51,** 14103 (1995).
2. R. M. Kusters, J. Singleton, D. A. Keen, R. McGreevy, and W. Hayes, *Physica B* **155,** 363 (1989).
3. Z. Zuotao and R. Yufang, *J. Solid State Chem.* **121,** 138 (1996).
4. A. Maignan, C. Simon, V. Caignaert, and B. Raveau, *J. Magn. Magn. Mater.* **152,** L5 (1996).
5. R. von-Helmolt, J. Wecker, T. Lorenz, and K. Samwer, *Appl. Phys. Lett.* **67,** 14 (1995).
6. Y. Moritomo, A. Asamitsu, H. Kuwahara, and Y. Tokura, *Nature* **380,** 141 (1996).
7. S. N. Ruddlesden and P. Popper, *Acta Crystallogr.* **11,** 541 (1958).
8. R. Seshadri, C. Martin, A. Maignan, M. Hervieu, B. Raveau, and C. N. R. Rao, *J. Mater. Chem.* **6,** 1585 (1996).
9. P. D. Battle, S. J. Blundell, M. A. Green, W. Hayes, M. Honold, A. K. Klehe, N. S. Laskey, J. E. Millburn, L. Murphy, M. J. Rosseinsky, N. A. Samarin, J. Singleton, N. A. Sluchanko, S. P. Sullivan, and J. F. Vente, *J. Phys.: Condensed Matter* **8,** L427 (1996).
10. P. D. Battle, S. J. Blundell, D. E. Cox, M. A. Green, J. E. Millburn, P. G. Radaelli, M. J. Rosseinsky, J. Singleton, L. E. Spring, and J. F. Vente, MRS Symposium Proceedings, Vol. 453, p. 331, 1997.
11. J. F. Mitchell, D. N. Argyriou, J. D. Jorgensen, D. G. Hinks, C. P. Potter, and S. D. Bader, *Phys. Rev. B* **55,** 63 (1997).
12. P. D. Battle, D. E. Cox, M. A. Green, J. E. Millburn, L. E. Spring, P. G. Radaelli, M. J. Rosseinsky, and J. F. Vente, *Chem. Mater.* **9,** 1042 (1997).
13. P. D. Battle, M. A. Green, N. S. Laskey, J. E. Millburn, P. Radaelli, M. J. Rosseinsky, S. P. Sullivan, and J. F. Vente, *Phys. Rev. B* **54,** 15967 (1996).
14. P. D. Battle, J. E. Millburn, M. J. Rosseinsky, L. E. Spring, J. F. Vente, and P. G. Radaelli, *Chem. Mater.* **9,** 3136 (1997).
15. P. D. Battle, M. A. Green, N. S. Laskey, N. Kasmir, J. E. Millburn, L. E. Spring, S. P. Sullivan, M. J. Rosseinsky, and J. F. Vente, *J. Mater. Chem.* **7,** 977 (1997).
16. P. D. Battle, J. Hepburn, J. E. Millburn, P. G. Radaelli, M. J. Rosseinsky, L. E. Spring, and J. F. Vente, *Chem. Mater.* **9,** 3215 (1997).
17. P. D. Battle, M. A. Green, N. S. Laskey, J. E. Millburn, M. J. Rosseinsky, S. P. Sullivan, and J. F. Vente, *Chem. Commun.* 767 (1996).
18. P. D. Battle, M. A. Green, N. S. Laskey, J. E. Millburn, L. Murphy, M. J. Rosseinsky, S. P. Sullivan, and J. F. Vente, *Chem. Mater.* **9,** 552 (1997).
19. P. A. Stadelman, *Ultramicroscopy* **21,** 131 (1987).
20. R. Seshadri, M. Hervieu, C. Martin, A. Maignan, B. Domenges, and B. Raveau, *Chem. Mater.* **9,** 1778 (1997).
21. P. Laffez, G. VanTendloo, R. Seshadri, M. Hervieu, C. Martin, A. Maignan, and B. Raveau, *J. Appl. Phys.* **80,** 5850 (1996).
22. H. Y. Hwang, S. W. Cheong, N. P. Ong, and B. Batlogg, *Phys. Rev. Lett.* **77,** 2041 (1996).